Progress In Electromagnetics Research C, Vol. 126, 23–37, 2022

Band-Stop Filtering for Electromagnetic Interference Rejection in Printed UWB Components Using Single Compact Archimedean Spiral EBG Cell

Sumon Modak[1], Partha P. Shome[1], Md. Ahsan Halimi[2], Taimoor Khan[2, *], Ahmed A. Kishk[3], and Tayeb A. Denidni[4]

Abstract—The design and analysis of a compact printed Archimedean spiral electromagnetic bandgap (EBG) structure are presented for frequency shielding in microwave circuits, including antenna and bandpass filters. The EBG characterization resonating at 7.7 GHz is done through a performance matrix such as transmission and reflection coefficients and equivalent circuit modeling, which demonstrates excellent resonance stability. The EBG unit cell is investigated for achieving frequency rejection in the printed monopole-based ultra-wideband (UWB) antenna and bandpass filter circuits. By introducing the Archimedean EBG unit cell on the UWB antenna ground plane, dual-frequency rejection, at 7.4, and 7.7 GHz, was realized. Further, such a structure is utilized in a multi-mode resonator (MMR) based UWB bandpass filter to attain band-notched functionality at 7.6 and 7.8 GHz with maximum attenuation of −16.5 and −15.6 dB, respectively. The prototypes of the EBG-loaded UWB antenna and EBG-Loaded UWB filter are fabricated and characterized. Excellent agreement is achieved between simulated and measured results of both prototypes.

1. INTRODUCTION

Ultra-wideband (UWB) technology has evolved as a potential solution for achieving a high data rate in modern wireless communication systems by virtue of its numerous advantages like wide operational bandwidth, low cost, low energy consumption, and lower system complexity [1]. UWB system is defined as a fractional bandwidth (BW) of more than 20% and a 500 MHz minimum bandwidth at the center frequency of their operating bandwidth. In 2002, to meet the growing popularity and demand for uniform regulatory guidelines for UWB systems, a 7.5 GHz band was released ranging from 3.1 to 10.6 GHz for commercial unlicensed UWB communications [2]. Since then, the research in UWB has seen manifold advancements targeting different functional modules and connectivity solutions. Antennas and bandpass filters (BPFs) constitute two important functional components of UWB systems. Consequently, they have drawn substantial attention among researchers amidst the different components used in the UWB transceiver systems. However, being the key functional units of the UWB front-end systems, designing the antennas and filters still holds different technical challenges like compact dimensions, good impedance matching, and omnidirectional radiation patterns [3–5]. Consequently, to achieve these UWB technology comes into existence, which offers high speed communications in consumptions of low power [6]. Similarly, for achieving high frequency selectivity in UWB systems BPFs play an important role by rejecting unwanted frequencies and improving the system performances [7, 8].

Received 24 August 2022, Accepted 14 October 2022, Scheduled 26 October 2022
* Corresponding author: Taimoor Khan (ktaimoor@ieee.org).
[1] Department of Electronics and Communication Engineering, Dr. B. R. Ambedkar National Institute of Technology, Jalandhar, Punjab, India. [2] Department of Electronics and Communication Engineering, National Institute of Technology Silchar, Assam, India. [3] Department of Electrical and Computer Engineering, Concordia University, Montreal, Canada. [4] INRS, University of Quebec, Canada.

To satisfy the Federal Communications Commission (FCC) regulations for unlicensed communication, the UWB filters are expected to have an ultra-wide passband with low insertion loss (IL) characteristics and uniform group delay (GD) variation [9]. Although UWB systems provide wide operational bandwidth, they are prone to signal interferences from different narrowbands like WiMAX (3.3–3.7 GHz), WLAN (5.15–5.35 GHz and 5.725–5.825 GHz), C-band satellite downlink and uplink (3.77–4.2 GHz and 5.925–6.425 GHz), and X-band satellite downlink and uplink (7.25–7.75 GHz and 8.025–8.4 GHz). Within the designated UWB, this signal interference causes degradation of the transmitted/-received signals [10, 11]. Hence, several efficient and economical techniques are realized and discussed in Section 2 to reject these interfering frequencies.

2. EMI REJECTIONS IN UWB CIRCUITS

UWB antennas and filters with band-notched characteristics are desired to reject unwanted electromagnetic interferences from different designated narrow band systems [12]. Traditionally, an antenna or a filter is accompanied by an additional narrowband filtering circuit for realizing the frequency rejection characteristic at specific frequencies. However, this conventional approach requires a narrowband resonator followed by its integration through an additional individual design of antenna or filter along with the narrowband resonator followed by its integration through an additional matching network. This approach adds a degree of design complexity and increases the overall system size [13]. Therefore, various alternative methods were invented and realized to develop UWB systems with inherent filtering features [14–22]. One of the methods to generate band-notched behavior in UWB antennas is by slotting the radiator or the ground plane of the antenna [14–17], or by introducing parasitic and resonators close to the antenna radiating element [18–22]. By implementing complementary split-ring resonators (CSRRs) without tampering with the radiator or the ground plane and generating any spurious radiation, a unique approach to realizing band-notch characteristics in UWB antennas is also studied in [23, 24]. Similarly, implementing a slotted line structure [25], open-loaded stub [26], and complimentary ring resonator CRR [27] in a UWB BPF stop-band characteristics can be realized. Some other resonators can be implemented to introduce band-notch characteristics in UWB filters. Guan [28] proposed UWB BPFs using a stepped-impedance slot-line resonator to generate a single notch at 5.2 GHz. Likewise, novel configurations of two UWB planar filters with stopband behavior are designed using a cross-coupled structure [29] and radial-loaded stub resonator [30], respectively. However, these techniques [14–30] have some constraints in notched width controlling capabilities affecting the current distribution in the passband frequencies. As a result, the time-domain performance and radiation pattern may be influenced. To overcome these challenges, recently, EBG structures have been widely accepted in the researchers' community for achieving the necessary frequency shielding in UWB antenna and filter designs. The EBG structures are periodic collections of dielectric and conductor material originating from the solid-state physics domain [31]. Around two decades ago, Yablonovitch designed a periodic structure by drilling holes in the dielectric material, creating a complete bandgap, in agreement with theoretical predictions [32]. Since then, EBG designs have become popular among researchers, and many EBG geometries have been investigated for electromagnetic shielding [33–36]. Extensive research work on UWB antennas loaded with EBG structures was reported in [37–45] for realizing EMI suppression. A miniaturized single band-notched UWB antenna is designed using a meander line EBG structure in [37] and C-slot EBG in [38]. Similarly, in [39], a compact UWB monopole antenna is designed to achieve dual-band rejection characteristics (5.2 and 5.8 GHz) using a dual inverted U-shaped slotted patch and edge located via EBG structure. A modified-EBG structure has been introduced for generating dual-notched bands at 3.5 and 5.5 GHz, respectively, in [40]. Mandal and Das developed a hexagon-shaped UWB monopole antenna with two mushroom EBG structures for realizing dual notched band characteristics [41]. Similarly, by introducing slitted EBG unit cells near the feedline, dual-notched band characteristics have been obtained for rejecting interference from WiMAX and WLAN bands [42]. In another interesting development, Majid et al. have designed a dual band-notched reconfigurable UWB antenna by implementing a U-shaped EBG structure [43]. Jaglan et al. [44] have optimized a defected ground compact EBG (DG-CEBG) structure to attain triple-notched behavior at WiMAX, WLAN, and X-band satellite communications. A multiband notched compact UWB antenna with EBG structures is reported in [45]. The proposed

antenna exhibits triple-notch-band behavior by incorporating three mushroom EBG structures coupled to the feed line. Similarly, notched band characteristics in UWB BPFs using EBG structures have also been realized, and the trend has been significantly increasing recently. Referenced designs [46–49] utilize various EBG structures over UWB BPFs for rejecting different interfering frequencies. Rotaru and Sykulski demonstrated a novel approach to creating a band-notched filter for avoiding interferences from the WLAN band (5.15–5.825 GHz) based on mushroom EBG structures [46]. Kurra et al. proposed a dual band-notched filter with frequency rejections at 5.19 GHz and 8.24 GHz, respectively, using uniplanar EBG structures [47]. A compact UWB BPF with dual narrow notched bands is presented in [48]. The notches (5.2 GHz and 5.8 GHz) are accomplished by introducing a pair of mushroom EBG structures near the feed line. In [49], an inverted U-shaped EBG structure has been utilized over the UWB bandpass filter for attaining dual-band notched characteristics at 2.4 GHz and 5.1 GHz for the applications in ISM and WLAN bands. The literature study shows that multiple EBG resonators must be implemented to realize multi-notch characteristics. However, the above-referenced antenna [37–45] and filter designs [46–49] produce multi-notched characteristics but suffer from large EBG dimensions. This becomes a limiting factor in realizing antenna or filter circuits of multi-notch functionality and compact dimensions. In the present work, a compact configuration of an EBG resonator, a miniaturized UWB monopole antenna, and a BPF are proposed to overcome such constraints. A compact single EBG unit cell is designed initially, and its corresponding performance parameters are discussed in detail. The EBG resonator is designed to exhibit a bandgap between 7.3 and 7.9 GHz and then integrated into the UWB antenna to accomplish dual rejection behavior at 7.4 and 7.7 GHz, respectively, as discussed in Section 4. Further, the same EBG structure is integrated with an MMR based UWB filter to obtain dual-notched band function at 7.6 and 7.8 GHz, as illustrated in Section 5. Furthermore, the simultaneous realization of dual-notched band functionality in antennas and filter circuits using the common EBG resonator has not been achieved till now. Section 6 discusses the experimental validation process of the proposed components. In Section 7, the comparison of the proposed work with existing literature is tabulated considering different EBG resonators, EBG loaded antennas, and EBG loaded filters, respectively.

3. PROPOSED EBG STRUCTURE FOR EMI REJECTION

In this section, the geometrical sketch of the perceived EBG unit cell and its performance characteristics are discussed. The design layout of the EBG unit cell is introduced in Fig. 1(a). Archimedean spiral resonators are conceptualized and extended from four square pads along with inter-digital lines arranged along the periphery of the EBG structure. The EBG resonator is etched on a Rogers RT duroid substrate (relative permittivity = 2.2 and thickness = 0.762 mm) and backed by a complete conductor surface. This unit cell has the optimized dimensions as: $B_1 = 3.12$ mm, $D_1 = D_2 = 0.66$ mm, $A_1 = A_2 = 0.12$ mm. Next, to identify the bandgap property of the proposed EBG resonator, the

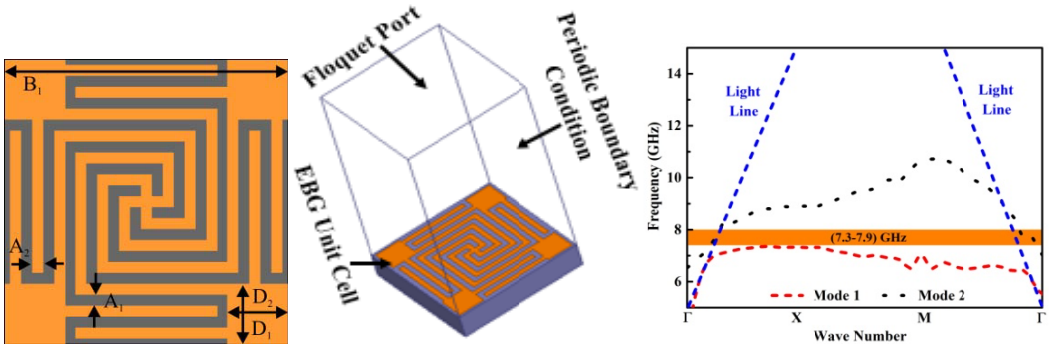

Figure 1. (a) Proposed EBG structure, (b) unit cell mode with a Floquet port, and (c) 2D-dispersion diagram.

dispersion diagram is computed using the Floquet theory in the FEM-based HFSS software. The simulation setup is represented in Fig. 1(b). The 2-D dispersion diagram for the proposed EBG structure is illustrated in Fig. 1(c). The horizontal axis indicates the transverse wave number calculated along an irreducible triangle in the Brillouin zone. Γ, X, and M represent three specific triangle points in the spectral domain. The bandgap dispersion curve for the proposed Archimedean EBG unit cell reveals stopband behavior within the frequency range of 7.3–7.9 GHz. Further, to investigate the physical phenomenon behind the EBG resonator, an equivalent circuit model is derived and implemented using Advanced Design System (ADS) tool. Fig. 2(a) reveals the equivalent circuit of the EBG unit cell coupled to a transmission line. For simplicity of understanding, the EBG resonator is divided into its constituent folded Archimedean spiral lines and inter-digital coupled resonator.

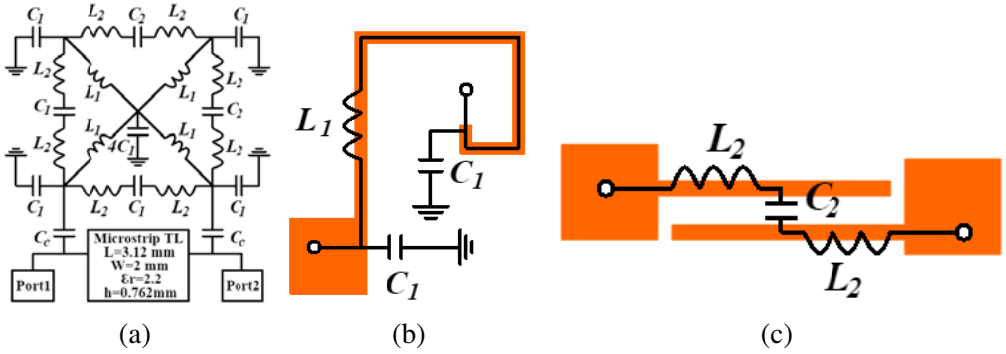

Figure 2. (a) EBG equivalent circuit model, (b) spiral metallic lines, and (c) inter-digital coupled lines with square pads.

The metallic part introduces the inductance in the circuit, whereas the capacitance is contributed by the intermediate gap between the inductive spiral lines and the peripheral inter-digital lines. The equivalent circuit of the folded metal lines section can be designed using inductor L_1 and parasitic shunt capacitor C_1 with respect to the ground. The values of L_1 and C_1 can be mathematically derived using Equation (1) and Equation (2) [50–52]. Two capacitors (Cc) are connected between the microstrip line and the unit cell (shown in Fig. 2(a)) to represent the coupling capacitance, and the microstrip line of length 3.12 mm is placed to account for the phase.

$$L_1 = 2l\left(\log\frac{l}{w} + 1.19 + 0.22\frac{w}{l}\right) \tag{1}$$

$$C_1 = 16.67 \times 10^{-4} l \frac{\sqrt{\varepsilon_{reff}}}{z_0} \tag{2}$$

Here l and w are the total length and width of the strip line, respectively. ε_{reff} is the effective dielectric constant, and Z_o is the impedance of the strip. The values of ε_{reff} and Z_o can be calculated using Equations (3) and (4), respectively.

$$\varepsilon_{reff} = \frac{\varepsilon_r + 1}{2} + \frac{\varepsilon_r - 1}{2}\left[\left(1 + 12\frac{h}{w}\right)^{-0.5} + 0.04\left(1 - \frac{w}{h}\right)^2\right] \tag{3}$$

$$Z_0 = \frac{120\pi}{2\pi\sqrt{\varepsilon_{reff}}} \ln\left(\frac{8h}{w} + 0.25\frac{w}{h}\right) \tag{4}$$

$$L_2 = 2l\left(\log\frac{l}{w} + 1.19 + 0.22\frac{w}{l}\right) \tag{5}$$

$$C_2 = 8.854 \times 10^{-6}\frac{\epsilon_r A(n-1)}{d} \tag{6}$$

Next, Fig. 2(c) shows the inter-digital line section of the EBG structure. It possesses some inductive effect (L_2) from the microstrip line and the inter-digital lines parallel plate capacitor (C_2). The

inductive part can be calculated using Equation (5), while the capacitor value can be determined using Equation (6) [53–55]. Here 'A' is the area occupied by the overlapped part, and 'd' is the gap between individual inter-digital lines. Finally, using the above two equations, the optimized values of $L_1 = 2.608\,\text{nH}$, $C_1 = 0.0557\,\text{pF}$, $L_2 = 0.6588\,\text{nH}$, $C_2 = 28.04947\,\text{pF}$, and $C_C = 0.6165\,\text{pF}$, are obtained, and its simulated $|S_{11}|$ curve is compared with the HFSS result in Fig. 3.

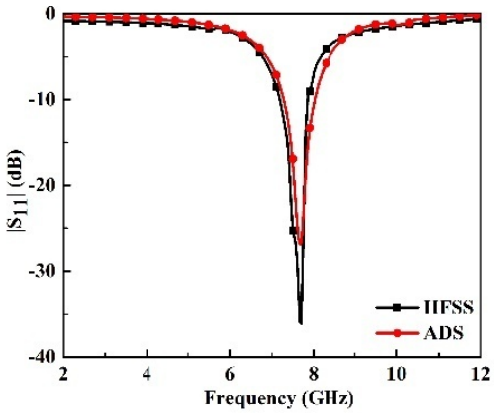

Figure 3. Simulated performance of equivalent circuit model and EBG resonator.

4. EBG-LOADED DUAL-BAND NOTCHED ANTENNA

This section discusses the design methodology and operating mechanism of the EBG loaded dual band-notched antenna for interference suppression in UWB systems. The miniaturized EBG resonator, introduced in Section 3, is implemented for notch generation in a UWB antenna circuit.

4.1. Geometrical Description of EBG-Loaded UWB Antenna

The geometries of the proposed conventional UWB antenna along with the EBG-loaded UWB antenna are shown in Fig. 4. Both antenna structures are implemented on the same Rogers material. In the first step, a basic UWB antenna is designed and presented in Fig. 4(a), whose geometry comprises a stepped rectangular radiating element on top and a partial ground plane on the substrate's other side. The partial ground plane is used to excite the multi-resonance characteristics, whereas the stepped rectangular slots enhance the impedance matching of the UWB. The designed Archimedean spiral EBG unit cell is deployed in the ground plane as a slotted element to create the desired band-notch characteristic. The top- and bottom-views of the proposed antenna can be seen in Figs. 4(b) and 4(c),

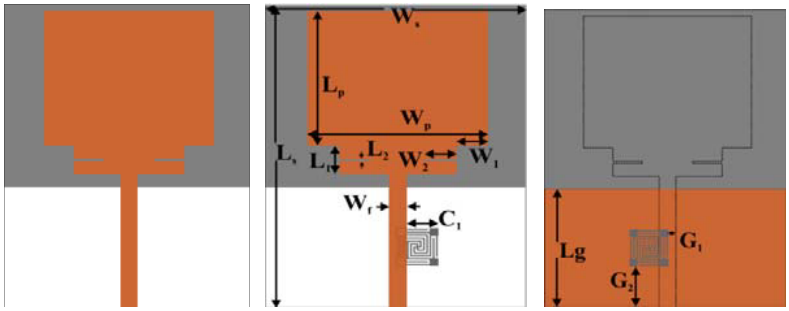

(a) (b) (c)

Figure 4. Proposed antenna structure, (a) conventional UWB antenna, (b) top-view of the dual-notched antenna, and (c) bottom-view of the dual-notched antenna.

respectively. The optimized dimensions (in mm) of the proposed design are $L_s = 36.8$, $W_s = 30$, $L_p = W_p = 20$, $W_f = 2$, $L_g = 15.1$, $W_1 = 3.5$, $L_1 = W_2 = 3.5$, $L_2 = 0.3$, $G_1 = 1.26$, $G_2 = 5.14$, $C_1 = 2.38$.

4.2. Performance Analysis of EBG-Loaded UWB Antenna

The antenna geometries, shown in Fig. 4, are designed and simulated using ANSYS HFSS software. Fig. 5(a) shows the simulated performance of the conventional UWB antenna and the proposed EBG-loaded UWB antenna. The reference antenna produces a wide impedance bandwidth of 8.1 GHz ranging from 2.6 to 10.7 GHz. Now, the suggested antenna defected with EBG structure on the right-hand side of the microstrip feed line exerts band-notched characteristics at 7.4 GHz (7.3–7.5 GHz) and 7.7 GHz (7.6–7.8 GHz), respectively, as illustrated in Fig. 5(a). Further, to validate the fidelity of the suggested design methodology, the same EBG unit cell is embedded on the left-hand side of the microstrip line. By virtue of the symmetrical nature of the UWB antenna geometry, identical antenna reflection characteristics are observed, and the corresponding graphical outcome is included in Fig. 5(a) for comparison. Moreover, to examine the effect of the truncated rectangular slots of the radiating element and the position of the EBG unit cell on the antenna performance, parametric analyses with respect to the geometrical parameters L_2, G_1, G_2 are carried out, and the associated variations are depicted in Figs. 5(b), 5(c), and 5(d), respectively. Here, the influence of all three associated design parameters in controlling the antenna performance can be observed, and accordingly, the dimensions and positions are selected to realize optimum antenna performance.

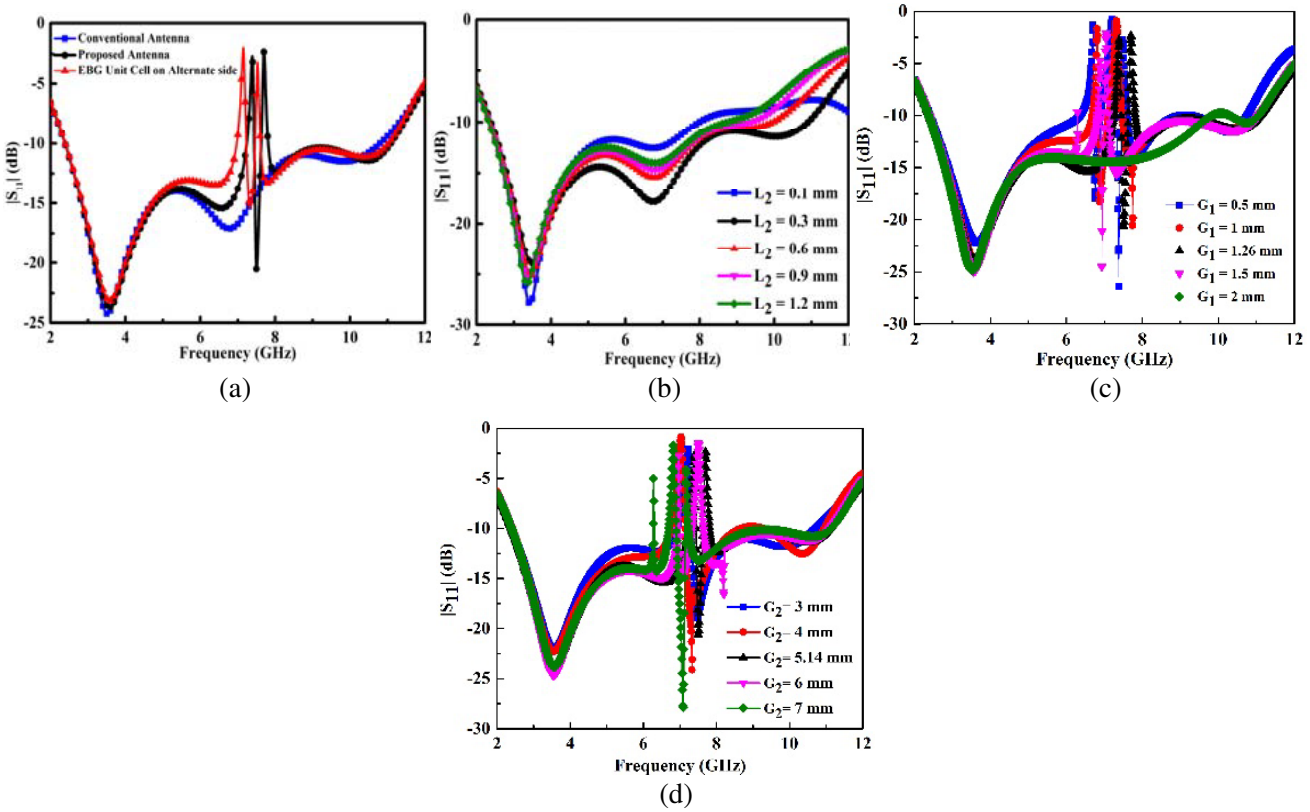

Figure 5. Simulated antenna performance, (a) $|S_{11}|$ comparison, (b) parametric variation of the parameter L_2, (c) parametric variation of the parameter G_1, and (d) parametric variation of the parameter G_2.

5. EBG-LOADED DUAL-BAND NOTCHED UWB FILTER

This section introduces the configuration of a UWB BPF with dual band-notched characteristics. By implementing the proposed Archimedean EBG unit cell in a UWB filter circuit, the MMR-based filtering capability of the EBG structure is verified for interference suppression in UWB communication.

5.1. Geometrical Description of EBG-Loaded UWB BPF

Figure 6 displays the geometrical configuration of the proposed EBG loaded dual band-notched UWB filter. A multi-mode resonating structure composed of a ring-shaped stub connected to a microstrip line is presented at the top layer of the proposed BPF. At the input and output sides of the proposed MMR configuration, inter-digital coupled lines are used to feed the proposed MMR configuration. The bottom layer contains the ground plane, which is defected by the EBG unit cell for creating the desired band-notch characteristics. The evolution of the suggested design involves conceptualizing a uniform impedance resonator (UIR) structure with inter-digital couple lines and then incorporating a circular ring-shaped open-ended stub at the center of the UIR to constitute the initial MMR-based UWB BPF. Next, the Archimedean spiral EBG unit cell is etched on the ground plane below the inter-digital coupled lines to generate the notch. This filter design is implemented on a Rogers RT duroid substrate. The optimized dimensions (in mm) are selected as: $L_1 = 7$, $L_{e1} = L_{e2} = 2.24$, $S_1 = S_2 = 0.2$, $C_1 = 0.52$, $E_1 = 2$, $E_2 = 1.9$, and $G_1 = 0.1$. Substrate-width (W_s) and substrate-length (L_s) are taken as 6 mm and 25.4 mm, respectively, and the dimensions of the EBG cell are kept unchanged.

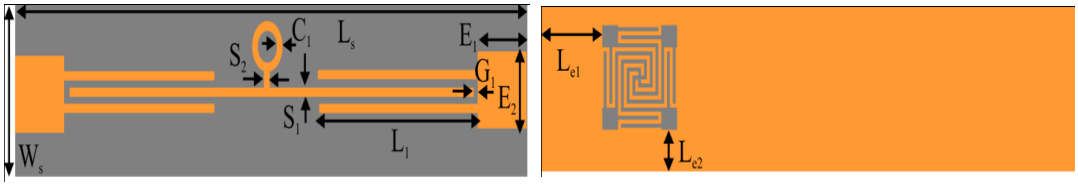

Figure 6. Geometrical configuration of (a) MMR-based UWB BPF, and (b) EBG-loaded dual-notched BPF.

5.2. Performance Analysis of EBG-Loaded UWB BPF

This section analyzes the performance of the MMR-based filter through a parametric study. At first, the resonance behavior of the conventional BPF is investigated. Weak coupling strength (L_1) is maintained across the MMR to determine the resonant frequencies. The MMR structure exerts dual resonance characteristics within the desired UWB operating band. Finally, the influence of the inter-digital coupled lines on the performance of the UWB filter is examined. To achieve stable passband characteristics, it is necessary to ensure strong coupling between the arms of the inter-digital lines and the MMR resonator. Fig. 7(a) shows the simulated frequency response for the suggested structure for different values of the coupling length (L_1), varying from 1 mm to 7 mm. Under weak coupling at $L_1 = 1$ mm, the dual resonances of the MMR can be witnessed. As L_1 increases, the transmission coefficient ($|S_{21}|$) curve flattens gradually. At $L_1 = 7$ mm, the necessary strong coupling is attained, and a uniform $|S_{21}|$ is achieved. Similarly, a parametric analysis with respect to C_1 (radius of circular ring-shaped stub), L_{e1}, and L_{e2} (Position of EBG unit cell) is investigated and shown in Fig. 7(b). It is evident that by varying the length of the MMR resonator, the locations of the two resonance frequencies can be adjusted simultaneously. On the other hand, the radius of the loaded circular stub can be used to tune the second resonant frequency of the MMR geometry. Further, the role of the EBG unit cell in obtaining the band-notched characteristics has been explored. The simulated frequency response displaying the reflection characteristics ($|S_{11}|$) and transmission characteristics ($|S_{21}|$) of the UWB filter, with and without the EBG unit cell, are plotted in Figs. 8(a) and 8(b), respectively. It can be observed that

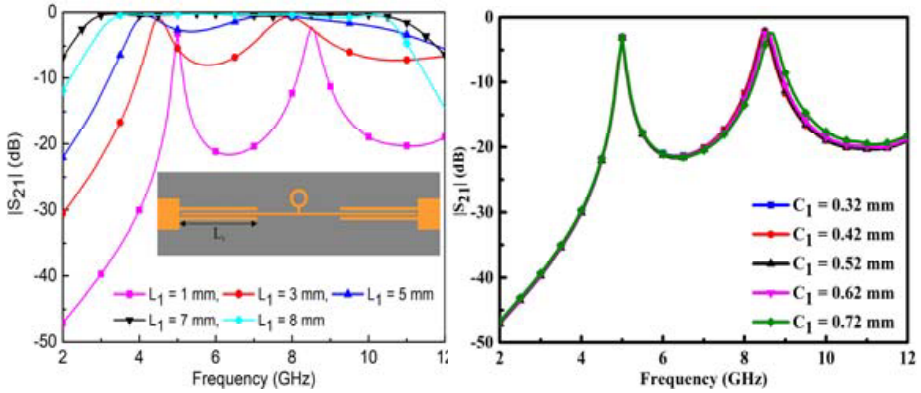

(a) (b)

Figure 7. $|S_{21}|$ variations of the UWB filter for (a) different coupled line lengths, (L_1), (b) different values of the radius of the loaded stub (C_s) at constant $L_1 = 1\,\text{mm}$.

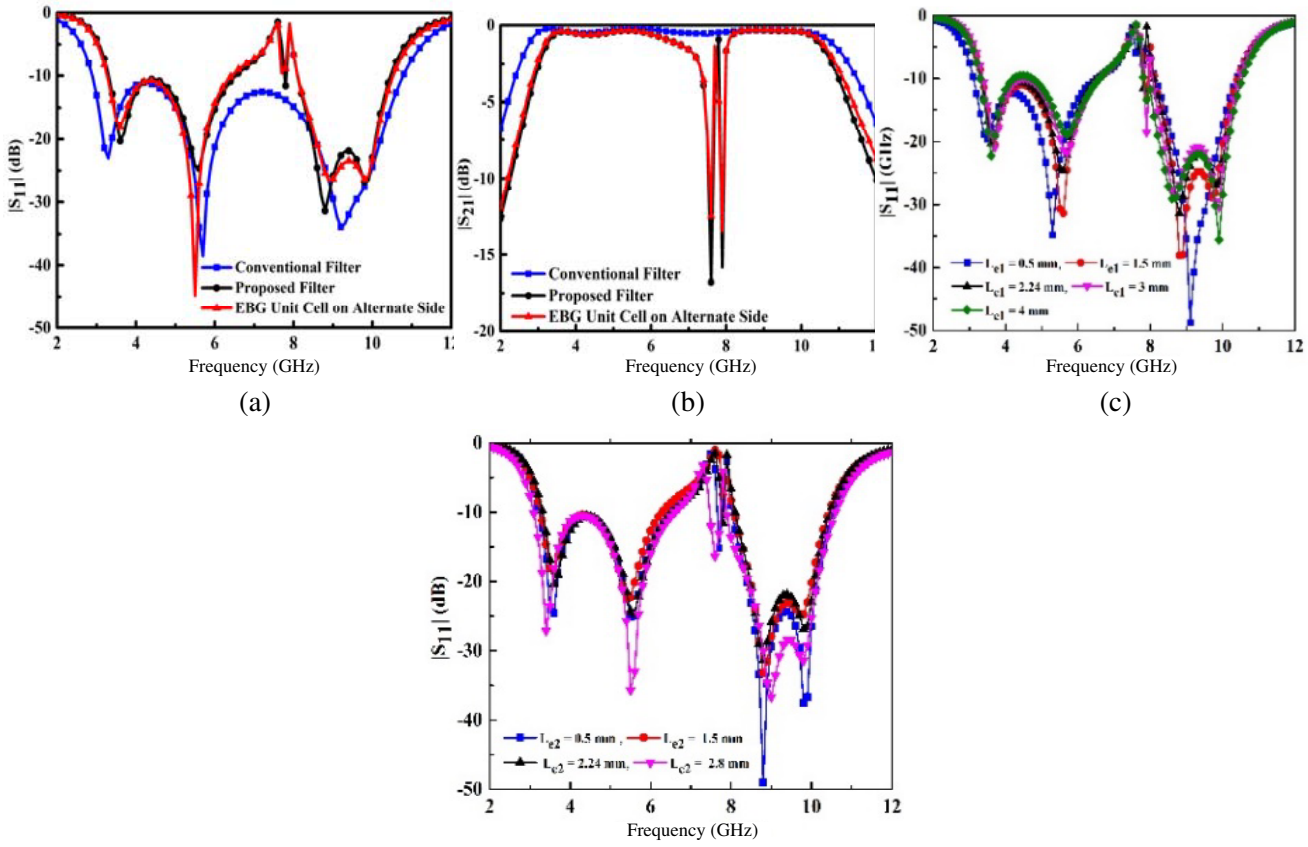

(a) (b) (c)

(d)

Figure 8. Simulated UWB filter performance characteristics (a) $|S_{11}|$, (b) $|S_{21}|$, parametric variation with respect to position to EBG unit cell (c) L_{e1} and (d) L_{e2}.

the impedance bandwidth of the initial MMR-based BPF ranges from 2.8 to 10.8 GHz with $|S_{11}|$ below $-30\,\text{dB}$.

The filters passband has three transmission poles at f_1, f_2, and f_3 = 3.3, 5.7, and 9.2 GHz, respectively. By embedding the EBG unit cell on the left side of the ground plane, the BPF produces dual notched band functions at 7.6 and 7.8 GHz, respectively. An almost identical frequency rejection

characteristic is witnessed for symmetrical incorporation of the EBG cell on the right side of the ground plane. It can be inferred that the frequency rejection capability is well retained in both cases. $|S_{21}|$ is noted to be uniform, around -1 dB within the operating bandwidth. However, attenuations of -16.5 dB and -15.6 dB are noticed at the two respective notch frequencies. It can now be concluded that in both cases, the same band rejection capability is retained, which is justified because of their symmetrical property. Further, a parametric analysis with respect to the position of the EBG unit cell is presented in Figs. 8(c), and 8(d), respectively. The performances of the EBG-loaded UWB antenna and EBG-loaded UWB filter are initially evaluated using simulation software. Next, prototypes are fabricated and measured using a vector network analyzer (VNA) to validate the design concept and simulated results experimentally. The experimental validation of the EBG-Loaded UWB antenna is discussed in Section 6.1. Likewise, Section 6.2 discusses the experimental validation of the EBG-Loaded UWB filter.

6. FABRICATIONS AND EXPERIMENTAL VALIDATION

6.1. Experimental Validation of EBG-Loaded UWB Antenna

The fabricated prototype for the proposed antenna design is presented in Fig. 9. The performance characteristics (simulated and measured) are shown in Fig. 10. It can be claimed that excellent agreement between measured and simulated results is achieved within the operating bandwidth and at the two-notched frequencies. A maximum gain of approximately 4 dBi at 8.2 GHz is observed, while the negative gain is obtained at the notch frequencies, as depicted in Fig. 10(b).

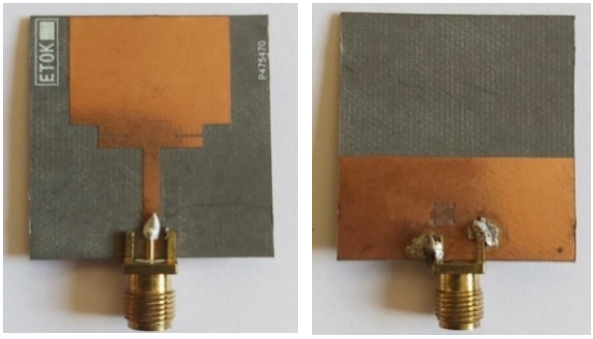

(a) (b)

Figure 9. Photos of the fabricated EBG-loaded antenna, (a) top-view, and (b) bottom-view.

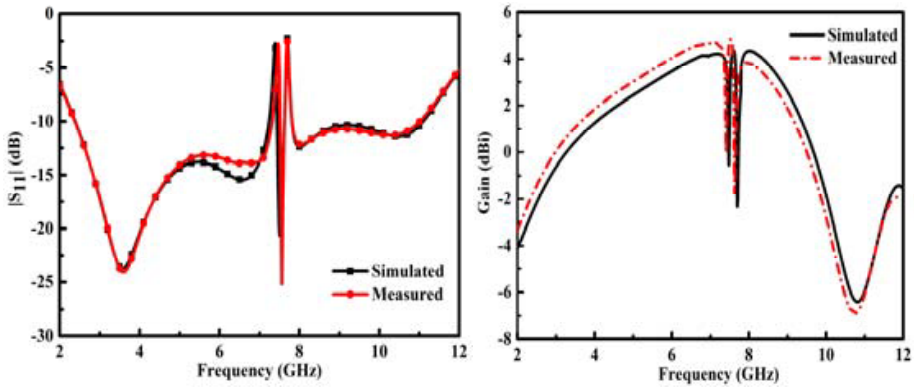

(a) (b)

Figure 10. Simulated and measured performance parameters for the proposed dual notched antenna, (a) $|S_{11}|$ comparison, and (b) gain comparison.

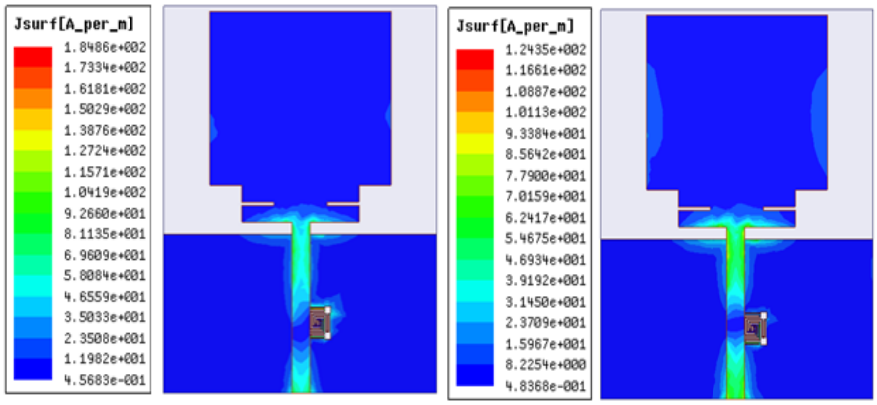

(a) (b)

Figure 11. Simulated surface current distribution (a) 7.4 GHz, and (b) 7.7 GHz.

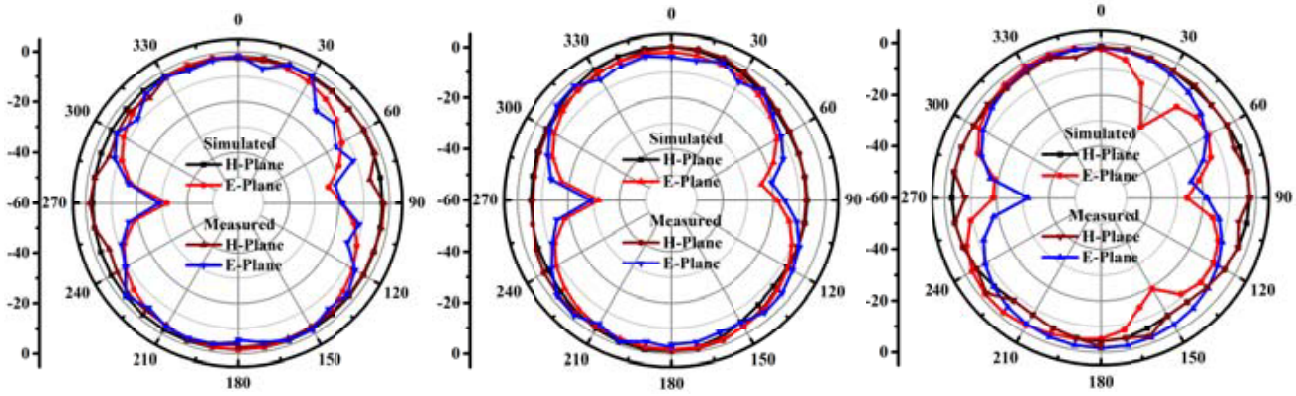

(a) (b) (c)

Figure 12. Simulated and measured 3D radiation characteristics of the band-notched antenna, (a) 3.5 GHz, (b) 7.5 GHz, and (c) 9.5 GHz.

The simulated surface current distributions at two different notches are plotted in Fig. 11, to better understand the working mechanism. It is seen that the strong surface current is retained by the EBG structure, which leads to the generation of two notches centered at 7.4 and 7.7 GHz, respectively. Fig. 12 outlines the simulated and measured radiation patterns for the suggested UWB antennas at three operating frequencies. It is seen that the H- and E-planes have monopole-like radiation patterns.

6.2. Experimental Validation of EBG-Loaded UWB BPF

Next, the miniaturized bandpass filter configuration is designed and fabricated to justify the feasibility of the proposed design. Fig. 13(a) shows the top view of the proposed design; meanwhile, Fig. 13(b)

(a) (b)

Figure 13. Photos of the fabricated prototype of the EBG-loaded BPF, (a) top-view, and (b) bottom-view.

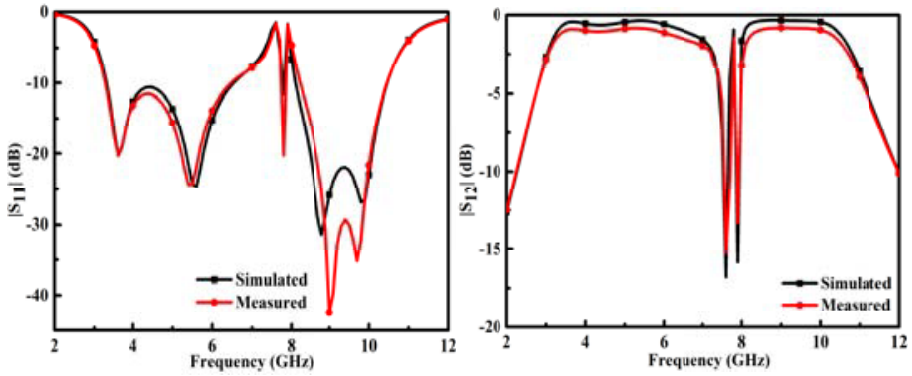

(a) (b)

Figure 14. Simulated and measured performance parameters (a) $|S_{11}|$, and (b) $|S_{21}|$.

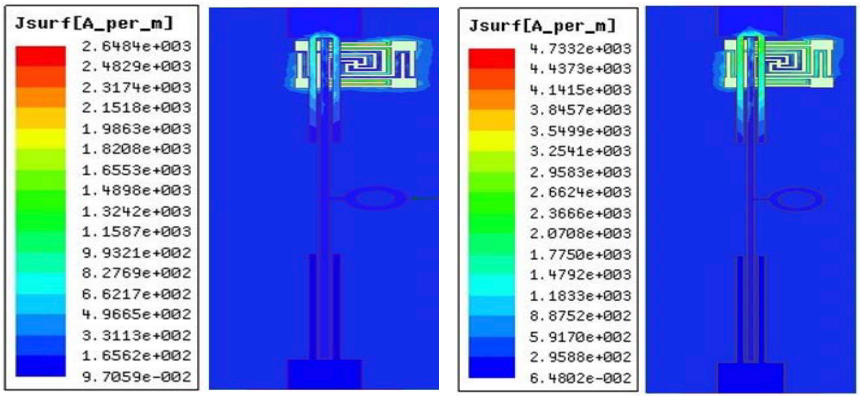

(a) (b)

Figure 15. Simulated surface current distribution (a) 7.6 GHz, and (b) 7.8 GHz.

shows the bottom view. The simulated and measured performances, in terms of reflection coefficient ($|S_{11}|$) and transmission coefficient ($|S_{21}|$), are plotted in Fig. 14. The measured $|S_{11}|$ values support dual-band rejection characteristics and match the simulated counterpart. In Fig. 15, the simulated surface current orientation at the notched frequencies indicates the role of EBG in introducing filtering behavior.

7. COMPARISON WITH EXISTING LITERATURE

A comparison with the existing literature has been conducted to identify the advantages of the proposed work. First, a comparison of the EBG unit cell is performed by considering the resonating frequency of the EBG unit cell. Simultaneously, the electrical size of the unit cells has been calculated and tabulated in Table 1 [33–36]. Also, a comparison with the literature on EBG embedded band-notched antennas is shown in Table 2. The comparison is based on notched frequencies. It is observed that designing SC-ML-EBG [33] and Koch Fractal EBG [34] structures is very difficult. Moreover, the SC-ML-EBG structure has a larger circuit area. It is further observed that using the TVS-EBG structure in [35] and the circular EBG structure in [36] adds to the design complexity because of their requirement of maintaining a periodic arrangement of the EBG unit cells.

Next, the performance of the proposed EBG-loaded UWB antenna is compared with the published designs available in [37–45] in terms of notched frequency and overall dimensions. Meander line EBG [37] and C-shaped slot EBG [38] can produce single-notched band characteristics. It is further observed that in [39–43], dual-notches have been obtained using different types of EBG structures. However,

Table 1. Comparison of the proposed EBG structure with existing literature.

Ref.	EBG Structures	ε_r	f_r (GHz)	Overall Size of EBG
[33]	SC-ML-EBG	2.65	2.5	$0.06\lambda_0 \times 0.06\lambda_0 \times 0.012\lambda_0$
[34]	Koch Fractal EBG	10.2	4.2	—
[35]	TVS-EBG	4.4	5.08	$0.11\lambda_0 \times 0.11\lambda_0 \times 0.012\lambda_0$
[36]	Circular EBG	10.2	8.5	—
Proposed EBG	**Archimedean Spiral EBG**	**2.2**	**7.7**	$\mathbf{0.08\lambda_0 \times 0.08\lambda_0 \times 0.019\lambda_0}$

f_r: Resonance frequency

Table 2. Comparison of the EBG-loaded antenna with existing literature.

Ref.	EBG-Loaded Technique	Notches	EBG unit cell size (mm^2)	f_n (GHz)	Overall Size of antenna (mm^3)
[37]	Meander Line EBG	1	$4.32 \times 4.32\,(= 18.0)$	5.2	$20.55 \times 44.45 \times 0.762\,(= 696)$
[38]	C-shaped slot EBG	1	$5.5 \times 5.5\,(= 30)$	5.2	$40 \times 40 \times 2\,(= 3200)$
[39]	U-Slot EBG	2	$4.45 \times 4.45\,(= 19.8)$	5.2/5.8	$35 \times 39 \times 0.813\,(= 1109.7)$
[40]	M-EBG	2	$8.2 \times 8.2\,(= 67.2)$	3.5/5.5	$30 \times 40 \times 1.6\,(= 1920)$
[41]	Mushroom EBG	2	$4.7 \times 4.7\,(= 22)$	3.5/5.5	$52 \times 32 \times 1.59\,(= 2645)$
[42]	Slitted-EBG	2	$10 \times 8\,(= 80)$	3.5/5.5	$40 \times 30 \times 1.6\,(= 1920)$
[43]	U-Shaped EBG	2	NA	3.9/5.5	$40 \times 80 \times 1.52\,(= 4864)$
[44]	DG-CEBG	3	$3 \times 3\,(= 9)$	3.4/5.5/7.6	$58 \times 45 \times 1.6\,(= 4176)$
[45]	Mushroom EBG	3	$5.6 \times 5.6\,(= 31.36)$	3.4/4.6/5.5	$50 \times 42 \times 1.6\,(= 3360)$
Proposed Antenna	**Archimedean Spiral EBG**	**2**	$\mathbf{3.12 \times 3.12\,(= 9.73)}$	**7.3/7.7**	$\mathbf{30 \times 36.8 \times 0.762\,(= 841.3)}$

f_n: Notched frequency

Table 3. Comparison of the proposed EBG-loaded bandpass filters with existing literature.

Ref.	EBG-Loaded Technique	Notches	EBG unit cell size (mm^2)	f_n (GHz)	Overall Size of filter (mm^3)
[46]	Mushroom EBG	1	$5.5 \times 5.5\,(= 30.25)$	5.4	$2 \times 5 \times 0.508\,(= 5.08)$
[47]	Uniplanar EBG	2	$4.32 \times 4.32\,(= 11.66)$	5.1/8.2	—
[48]	Mushroom EBG	2	$4.2 \times 4.2\,(= 17.64)$	5.2/5.8	$32 \times 20 \times 1\,(= 640)$
[49]	Inverted U-Shaped EBG	2	—	2.4/5.1	$19 \times 53 \times 0.127\,(= 127)$
Proposed Filter	**Archimedean Spiral EBG**	**2**	$\mathbf{3.12 \times 3.12\,(= 9.73)}$	**7.6/7.9**	$\mathbf{6 \times 25.4 \times 0.762\,(= 116)}$

f_n: Notched frequency

the overall antenna size is too large compared to the proposed EBG-loaded UWB antenna. In [44], a DG-CEBG structure has been used for producing triple-notched bands. However, its design size is too large compared to the proposed one. Mushroom EBG structures [45] generate triple-notched band characteristics with large circuit dimensions. A comparison is also made based on the EBG-loaded UWB filters, as illustrated in Table 3. It is seen that the mushroom EBG structure in [46] has a compact size but fails to produce an adequate number of notches. Likewise, uniplanar EBG [47], mushroom EBG [48], and inverted U-shaped EBG [47] have also been used for dual-band rejection, though the EBG structures in [48, 49] produce dual-notched band functions achieving design compactness. Finally, it can be concluded that the suggested Archimedean spiral EBG structure possesses a novel geometry with a compact dimension. In addition, the single EBG unit cell can produce dual-notched band characteristics in both EBG-loaded UWB antenna and EBG-loaded UWB filter, which is advantageous.

8. CONCLUSION

This investigation has presented a detailed analysis of the implementation of an EBG structure to realize electromagnetic interference suppression in microwave circuits. An Archimedean Spiral EBG unit cell has been designed with a bandgap characteristic. An in-depth analysis of the EBG resonator has also been carried out to optimize the dimensions to achieve the desired performance. Next, by introducing the proposed Archimedean EBG unit cell on the ground plane of the UWB antenna, dual-frequency rejection characteristics at 7.4 GHz and 7.7 GHz have been realized. A dual notch band characteristic has been retained at the center frequencies of 7.6 GHz and 7.8 GHz, respectively, by implementing the same EBG structure in a compact UWB filter. The efficient performance matrix realized within the operating bandwidth of both designs (antenna and filter) establishes them as excellent candidates for UWB applications.

REFERENCES

1. Ray, K. P., "Design aspects of printed monopole antennas for ultra-wideband applications," *International Journal of Antennas and Propagation*, Vol. 2008, Article ID 713858, 1–9, 2008.
2. Federal Communications Commission, "Revision of Part 15 of the Commission's rules regarding ultra-wideband transmission systems," First Report and Order, FCC 02-48, Washington, DC, 2002.
3. Cicchetti, R., E. Miozzi, and O. Testa, "Wideband and UWB antennas for wireless applications: A comprehensive review," *International Journal of Antennas and Propagation*, Vol. 2017, Article ID 2390808, 1–46, 2017.
4. Hao, Z. and J. Hong, "Ultra wideband filter technologies," *IEEE Microwave Magazine*, Vol. 11, No. 4, 56–68, 2010.
5. Fan, S.-T., Y.-Z. Yin, H. Li, and L. Kang, "A novel self-similar antenna for UWB applications with band-notched characteristics," *Progress In Electromagnetics Research Letters*, Vol. 22, 1–8, 2011.
6. Dastranj, A., "Optimization of a printed UWB antenna: Application of the invasive weed optimization algorithm in antenna design," *IEEE Antennas and Propag. Magazine*, Vol. 59, No. 1, 48–57, 2017.
7. Wang, L. T., Y. Xiong, and M. He, *Review on UWB Bandpass Filters, UWB Technology — Circuits and Systems*, M. Kheir, Intech Open, 2019.
8. Dardeer, O. M., H. A. Elsadek, H. M. Elhennawy, and E. A. Abdallah, "Ultra-wideband bandstop filter with multi transmission zeros using in-line coupled lines for 4G/5G mobile applications," *AEU-International Journal of Electronics and Communications*, Vol. 131, 1–6, 2021.
9. Shome, P. P., T. Khan, S. K. Koul, and Y. M. M. Antar, "Two decades of UWB filter technology: Advances and emerging challenges in the design of UWB bandpass filters," *IEEE Microwave Magazine*, Vol. 22, No. 8, 32–51, 2021.
10. Modak, S., T. Khan, T. A. Denidni, and Y. M. M. Antar, "Miniaturized self-isolated UWB MIMO planar/cuboidal antenna with dual X-band interference rejection," *AEU-International Journal of Electronics and Communications*, Vol. 143, 1–6, 2022.
11. Shome, P. P., T. Khan, and R. H. Laskar, "A state-of-art review on band-notch characteristics in UWB antennas," *Int. Journal of RF and Microwave Comp. Aided Engg.*, Vol. 29, No. 2, 1–16, 2018.
12. Modak, S., T. Khan, and R. H. Laskar, "Loaded UWB monopole antenna for quad band-notched characteristics," *IETE Technical Review*, Vol. 39, 1–9, 2021.
13. Xu, J., et al., "A small UWB antenna with dual band-notched characteristics," *International Journal of Antennas and Propagation*, Vol. 2012, Article ID 656858, 2012.
14. Emadian, S. R., C. Ghobadi, J. Nourina, M. H. Mirmozafari, and J. Pourahmadaza, "Bandwidth enhancement of CPW-fed circle-like slot antenna with dual band-notched characteristics," *IEEE Antennas Wireless Propag. Lett.*, Vol. 11, 543–546, 2012.

15. Modak, S. and T. Khan, "A slotted UWB-MIMO antenna with quadruple band-notch characteristics using mushroom EBG structure," *AEU-International Journal of Electronics and Communications*, Vol. 134, 1–6, 2021.
16. Lui, W., C. Cheng, and H. Zhu, "Improved frequency notched ultra wideband slot antenna using square ring resonator," *IEEE Antennas Wireless Propag. Lett.*, Vol. 55, No. 9, 2445–2450, 2007.
17. Peddakrishna, S. and T. Khan, "Design of UWB monopole antenna with dual notched band characteristics by using π-shaped slot and EBG resonator," *AEU-International Journal of Electronics and Communication*, Vol. 96, 107–112, 2018.
18. Azim, R., M. T. Islam, and A. T. Mobashsher, "Dual band-notch UWB antenna with single tri-arm resonator," *IEEE Antennas Wireless Propag. Lett.*, Vol. 13, 670–373, 2014.
19. Ryu, K. S. and A. A. Kishk, "UWB antenna with single or dual band-notches for lower WLAN band and upper WLAN band," *IEEE Transactions on Antennas and Propagation*, Vol. 57, No. 12, 3942–3950, 2009.
20. Sabouni, A. and A. A. Kishk, "Single or multi notch bands applied to microstrip excited ultra-wideband antennas with dielectric resonator antenna case," *Microw. Opt. Technol. Lett.*, Vol. 55, No. 5, 1066–1069, 2013.
21. Yadav, D., M. P. Abegaonkar, S. K. Koul, V. Tiwari, and D. Bhatnagar, "A compact dual band-notched UWB circular monopole antenna with parasitic resonators," *AEU-International Journal of Electronics and Communications*, Vol. 84, 313–320, 2018.
22. Salamin, M. A., W. A. E. Ali, S. Das, and A. Zugari, "Design and investigation of a multi-functional antenna with variable wideband/notched UWB behaviour for WLAN/X-band/UWB and Ku-band applications," *AEU-International Journal of Electronics and Communications*, Vol. 111, 1–7, 2019.
23. Siddiqui, J. Y., C. Saha, and Y. M. M. Antar, "Compact SRR loaded UWB circular monopole antenna with frequency notch characteristics," *IEEE Transactions on Antennas and Propagation*, Vol. 62, No. 8, 4015–4020, 2014.
24. Siddiqui, J. Y., C. Saha, and Y. M. M. Antar, "Compact dual-SRR-loaded UWB monopole antenna with dual frequency and wideband notch characteristics," *IEEE Antennas Wireless Propag. Lett.*, Vol. 14, 100–103, 2015.
25. Guan, X., P. Gui, T. Xiong, B. Ren, and L. Zhu, "Hybrid microstrip/slot line ultra-wideband bandpass filter with controllable notch band," *International Journal of Antennas and Propagation*, 1–8, 2017.
26. Zheng, X., Y. Wang, and T. Jiang, "Compact band notched UWB filter based on open-load stub," *PIERS Proceedings*, 2844–2847, Prague, Czech Republic, Jul. 6–9, 2015.
27. El Omari El Bakali, H., et al., "A compact UWB bandpass filter with WLAN band rejection using hybrid technique," *Proc. of the International Conference Interdisciplinary in Engineering (INTER-ENG)*, 922–926, 2020.
28. Gaun, X., "Slot-line UWB bandpass filters and band-notched UWB filters," *UWB Technology and its Applications*, Chapter 3, 43–58, 2018.
29. Li, S. L. and W. B. Zeng, "Design of ultra-wideband filter with band-notched characteristic based on left-handed materials," *Proceedings of Asia Conf. on Power and Electrical Engineering*, 1–5, 2016.
30. Liu, C. Y., T. Jiang, J. Zhang, and Y. S. Li, "A novel UWB filter with notch-band characteristic using radial-loaded stub resonator," *Procedia Engineering*, Vol. 15, 2428–2433, 2011.
31. Yang, F. and Y. Rahmat-Samii, *Electromagnetic Band Gap Structures in Antenna Engineering*, Cambridge University Press, New York, 2009.
32. Yablonovitch, E., "Inhibited spontaneous emission in solid-state physics and electronics," *Phys. Rev. Lett.*, Vol. 58, 2059–2062, 1987.
33. Lin, B., X. Ye, X. Cao, and F. Li, "Uniplanar EBG structure with improved compact and wideband characteristics," *Electronics Letters*, Vol. 44, No. 23, 1362–1363, 2008.
34. Ruiz, J. D., F. L. Martinez, and J. Hinojosa, "Novel compact wide-band EBG structure based on tapered 1-D Koch fractal patterns," *IEEE Antennas Wireless Propag. Lett.*, Vol. 10, 1104–1107, 2011.

35. Bhavarthe, P. P., S. S. Rathod, and K. T. V. Reddy, "A compact two via slot-type electromagnetic bandgap structure," *IEEE Microwave and Wireless Components Letters*, Vol. 27, No. 5, 446–448, 2017.
36. Chiau, C. C., X. Chen, and C. Parini, "Multiperiod EBG structure for wide stopband circuits," *IEEE Proceedings — Microwaves, Antennas and Propagation*, Vol. 150, No. 6, 489–492, 2003.
37. Kurra, L., M. P. Abegaonkar, A. Basu, and S. K. Koul, "A band-notched UWB antenna using uni-planar EBG structure," *European Conf. on Antennas and Propagation (EuCAP)*, 2466–2469, Gothenburg, 2013.
38. Song, C. Y., T. Y. Yang, W. W. Lin, and X. L. Yang, "Design of a band-notched UWB antenna based on EBG structure," *IEEE Int. Conf. on Applied Superconductivity and Electromag. Devices*, 274–277, China, 2013.
39. Abdalla, M. A., A. Al-Mohamadi, and A. Mostafa, "Dual notching of UWB antenna using double inversed U-shape compact EBG structure," *International Congress on Advanced Electromagnetic Materials in Microwaves and Optics*, 1–3, 2016.
40. Liu, H. and X. Ziqiang, "Design of UWB monopole antenna with dual notched bands using one modified electromagnetic-bandgap structure," *Scientific World Journal*, Vol. 2013, 1–9, 2013.
41. Mandal, T. and S. Das, "Design of dual notch band UWB printed monopole antenna using electromagnetic bandgap structure," *Microw. Opt. Technol. Lett.*, Vol. 56, 2195–2199, 2014.
42. Mehdi, G., et al., "Miniaturized UWB antenna with dual-band rejection of WLAN/WiMAX using slitted EBG structure," *IET Microw. Antennas Propag.*, 360–366, 2019.
43. Majid, H. A., et al., "Reconfigurable band notch UWB antenna using EBG structure," *Proceedings of IEEE Asia-Pacific Conference on Applied Electromagnetic (APACE)*, 268–270, Johor Bahru, 2014.
44. Jaglan, N., S. D. Gupta, B. Kanaujia, S. Srivastava, and E. Thakur, "Triple band notched DG-CEBG structure based UWB MIMO/diversity antenna," *Progress In Electromagnetics Research C*, Vol. 80, 21–37, 2018.
45. Jaglan, N., B. Kanaujia, S. D. Gupta, and S. Srivastava, "Triple band notched UWB antenna design using electromagnetic band gap structures," *Progress In Electromagnetics Research C*, Vol. 66, 139–147, 2016.
46. Rotaru, K. and J. Sykulski, "Compact electromagnetic bandgap structures for notch band in ultra-wideband applications," *Sensors*, Vol. 10, 9620–9629, 2010.
47. Kurra, L., M. P. Abegaonkar, A. Basu, and S. K. Koul, "A compact uniplanar EBG structure and its application in band-notched UWB filter," *International Journal of Microwave and Wireless Technologies*, Vol. 5, 491–498, 2013.
48. Liu, B., Y. Yin, Y. Yang, S. Jing, and A. Sun, "Compact UWB bandpass filter with two notched bands based on electromagnetic bandgap structures," *Electronics Letters*, Vol. 47, No. 13, 757–758, 2011.
49. Venkatesh, M. N., M. Mandhe, B. N. Kumar, and K. C. S. Kavya, "Experimental design and illustration of narrow band compact microwave notch filter using EBG structure," *International Journal of Recent Technology and Engineering*, Vol. 7, No. 5, 1–9, 2019.
50. Mohajer-Iravani, B. and O. M. Ramahi, "Wideband circuit model for planar EBG structures," *IEEE Trans. Adv. Package*, Vol. 33, No. 1, 169–179, 2010.
51. Mohajer-Iravani, B. and O. M. Ramahi, "Electromagnetic interference reduction using electromagnetic bandgap structures in packages, enclosures, cavities, and antennas," 62–89, Dept. of Electrical and Computer Engineering, University of Maryland, Maryland, 2007.
52. Pozar, D. M., *Microwave Engineering*, 163–169, Wiley, New York, NY, 1997.
53. Bahl, I. J., *Lumped Elements for RF and Microwave Circuits*, Artech House, Norwood, MA, 2003.
54. Chaddock, R. E., "The application of lumped element techniques to high frequency hybrid integrated circuits," *Radio Electron. Eng.*, Vol. 44, No. 8, 414–420, 1974.
55. Kurra, L., M. P. Abegaonkar, and S. K. Koul, "Equivalent circuit model of resonant-EBG bandstop filter," *IETE Journal of Research*, 2015.